AD-A265 958

PL-TR-92-2106

CLOUD SCENE SIMULATION MODELING
THE ENHANCED MODEL

Maureen E. Cianciolo
R. Gary Rasmussen

TASC
55 Walkers Brook Drive
Reading, Massachusetts 01867

April 1992

Final Report
Period Covered: December 1989 – March 1992

DTIC
ELECTE
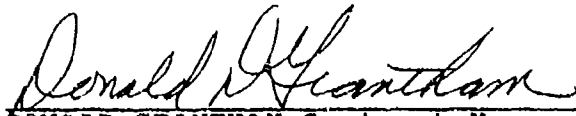JUN 1 4 1993
S E D

Approved for public release; distribution unlimited

PHILLIPS LABORATORY
Air Force Systems Command
Hanscom Air Force Base, Massachusetts 01731-5000

93-13146

"This technical report has been reviewed and is approved for publication"

[signature]

DONALD GRANTHAM Contract Manager
Chief, Atmospheric Structure Branch
Atmospheric Sciences Division

[signature]

ROBERT A. McCLATCHEY, Director
Atmospheric Sciences Division

This report has been reviewed by the ESC Public Affairs Office (PA) and is releasable to the National Technical Information Service (NTIS).

Qualified requestors may obtain additional copies from the Defense Technical Information Center. All others should apply to the National Technical Information Service.

If your address has changed, or if you wish to be removed from the mailing list, or if the addressee is no longer employed by your organization, please notify PL/TSI, Hanscom AFB, MA 01731-5000. This will assist us in maintaining a current mailing list.

Do not return copies of this report unless contractual obligations or notices on a specific document requires that it be returned.

REPORT DOCUMENTATION PAGE

1. AGENCY USE ONLY *(Leave blank)*	2. REPORT DATE April 1992	3. REPORT TYPE AND DATES COVERED Final Report December 1989 – March 1992

4. TITLE AND SUBTITLE Cloud Scene Simulation Modeling The Enhanced Model	5. FUNDING NUMBERS PE 62101F PR 6670 TA 09 WU BE Contract F19628-90-C-0022

6. AUTHOR(S) Maureen E. Cianciolo R. Gary Rasmussen	

7. PERFORMING ORGANIZATION NAME(S) AND ADDRESS(ES) TASC 55 Walkers Brook Drive Reading, MA 01867	8. PERFORMING ORGANIZATION REPORT NUMBER

9. SPONSORING/MONITORING AGENCY NAME(S) AND ADDRESS(ES) Phillips Laboratory Hanscom AFB, MA 01731-5000 Contract Manager: Donald Grantham/GPAA	10. SPONSORING/MONITORING AGENCY REPORT NUMBER PL-TR-92-2106

11. SUPPLEMENTARY NOTES

12a. DISTRIBUTION/AVAILABILITY STATEMENT Approved for public release; distribution unlimited	12b. DISTRIBUTION CODE

13. ABSTRACT *(Maximum 200 words)*

This report documents the development of the Enhanced Cloud Scene Simulation Model developed by TASC for Phillips Laboratory in support of the Smart Weapons Operability Enhancement (SWOE) Program under the Balanced Technology Initiative. The model simulates multi-dimensional cloud water density fields for input to radiative transfer models and scene generation systems. The enhanced cloud model incorporates additional capabilities and modifications to previous model versions. This document focuses on those new capabilities and briefly summarizes the technical tasks completed under the Cloud Scene Model Development Project.

14. SUBJECT TERMS Cloud model Fractal model Scene simulation Cumulus model	15. NUMBER OF PAGES 44
	16. PRICE CODE

17. SECURITY CLASSIFICATION OF REPORT Unclassified	18. SECURITY CLASSIFICATION OF THIS PAGE Unclassified	19. SECURITY CLASSIFICATION OF ABSTRACT Unclassified	20. LIMITATION OF ABSTRACT SAR

NSN 7540-01-280-5500
FS911
6-8-91

Standard Form 298 (Rev. 2-89)
Prescribed by ANSI Std 239-18
298-102

TABLE OF CONTENTS

Page

LIST OF FIGURES

LIST OF TABLES

v

1.   INTRODUCTION

1.1   PROJECT OVERVIEW

One goal of the SWOE Program is to enhance the operational capabilities of future smart weapons through more comprehensive consideration of the environment. A key element of the SWOE program is a planned sensor evaluation and test facility for millimeter wave and infrared sensors. Sensor studies will be carried out using both actual field data and simulated data. The purpose of the Cloud Scene Model Development project is to meet the latter objective by simulating realistic cloud fields for use in radiometric sensor evaluation studies as well as scene visualization. Two major efforts of the Cloud Scene Simulation project are model software development and applied research.

Model software development tasks include the design, implementation, integration, testing, documentation and delivery of two interim models and a final cloud model. Applied research tasks include the analysis of cloud data (specifically liquid water density) and a comparison of various synthetic field generation techniques. Results from these analyses are used in model development with the goal of producing physically and visually realistic cloud fields with computational efficiency.

The six technical tasks are outlined below.

Task 1   **MODEL DESIGN**

Analyze SWOE requirements. Design a stochastic cloud scene simulation model based on observed cloud morphology and atmospheric physics. Specify algorithms, data structures, data flows and software architecture. Define the software interface with other SWOE computer codes.

Task 2   **MODEL VERSION 1 (The Prototype Model)**

Rapidly implement, test and deliver a prototype cloud model based on the Boehm sawtooth wave technique for generation of random fields. Model stratiform cloud type only. Test software before delivery. Prepare a user guide.

Task 3 STUDIES AND ANALYSES

Survey recent scientific literature to identify prior investigations of the spatial and temporal variability of cloud water over geographical regions of interest. If necessary, locate, obtain and analyze empirical cloud data. Compare alternate field generation algorithms and determine model parameters which will result in cloud shapes and water distributions characteristic of stratiform, cumuliform and cirriform cloud types.

Task 4 MOᵢ ᵀL VERSION 2 (The Interim Model)

Refiᵣ. the prototype model based on the results of Task 3. Add the capability to generate cirriform cloud types. Implement the cloud shadow post-processor. Test prior to delivery. Prepare a user guide.

Task 5 SWOE COMPATIBILITY

Evaluate selected SWOE cloud history databases and radiative transfer models for compatibility with the cloud scene simulation model. Optimize the cloud shadow post-processor for typical SWOE usage.

Task 6 MODEL VERSION 3 (The Enhanced Model)

Refine the interim model using the knowledge gained in previous tasks. Develop a cumuliform cloud model, add temporal evolution and a variable-resolution grid option to the model. Implement a visualization post-processor to convert cloud model output fields to polygonal isosurfaces. Test software prior to delivery. Prepare a user guide.

The technical findings and conclusions drawn from Tasks 1 through 5 were discussed in a previous report (Ref. 1). In this report, we describe new developments culminating in the enhanced cloud model, Task 6.

Much of the overall design of the enhanced model is similar to the prototype and interim models developed previously and documented in Ref. 1. In that document we described the requirements analysis and design of the cloud model. Here we recreate the table that lists the SWOE requirements for the cloud scene simulation model and the corresponding model design decisions (Table 1). The enhanced model accommodates all of the requirements listed in the table and therefore replaces the prototype and interim models.

Those capabilities that were developed since Ref. 1 and are unique to the enhanced model are documented in detail in Section 2 of this report. They include: a variable-resolution output grid, a more flexible fractional Brownian motion model that allows for point-wise field evaluation, temporal evolution and a cumulus convection model.

Table 1   Overall SWOE Cloud Model Requirements and Design

	SWOE MODEL REQUIREMENTS	DESIGN DECISIONS
1	Produce realistic spatial and temporal distributions of cloud water (for stratiform, cirriform and cumuliform types) in the absence of real data.	Use stochastic algorithm.
2	Treat the complex structure of clouds for realism in radiometric sensor computations (e.g., cloud edge effects).	
3	Generate multiple scenes given identical meteorological input for sensitivity studies.	
4	Produce cloud fields in a computationally efficient manner.	
5	Generate high resolution cloud fields where necessary for use in radiometric computations and visualization (accommodate low resolution clouds on the horizon).	Incorporate variable resolution data grid.
6	Allow for a wide range of ground domain sizes and resolutions.	Use variable resolution grid to economize on memory storage requirements and simulate scenes on scales of 10-100 km.
7	Provide capability to generate scenes for a variety of sensor applications (e.g., top down, skimmer, air-to-air, etc.).	Generate fields that can be viewed from all angles. Include capability to produce scenes large enough to have clouds on the horizon.
8	Produce cloud scenes representative of any user-specified location and historical time.	Accept historical meteorological data as model input.
9	Generate model output in a form that can be used for radiometric sensor studies (both MMW and IR applications).	Produce liquid water density fields as output.
10	Integrate model with other SWOE simulation models.	Design model with replaceable interface module. Write all software in standard FORTRAN 77. Design model to be highly modular.
11	Provide polygonalized cloud scenes to ETL for visualization.	Implement polygon generation method with the capability to simulate colored cloud scenes (for additional realism).
12	Generate cloud shadow map for input to energy balance computations.	Provide a cloud shadow post-processor.

1.2   CLOUD MODEL OVERVIEW

The enhanced cloud scene simulation model uses stochastic field generation techniques and knowledge of atmospheric structure and physics to model four-dimensional (3 spatial and 1 temporal) cloud scenes. It simulates up to four cloud layers (low, middle, high and cumulus) including stratiform, cirriform and cumuliform cloud

types. Cloud scenes are representative (in a statistical sense) of specific environmental conditions provided by the user in the form of sounding data and cloud layer information. A description of the major procedures within the enhanced cloud model is provided in Ref. 2. Here we review the model logic.

A fractional Brownian motion model is used to simulate the two-dimensional horizontal distribution of cloud elements within each layer. We use the rescale and add (RSA) algorithm (Ref. 3). The RSA algorithm generates a stochastic field whose character is controlled by a few key model parameters. By applying a threshold to the field we can obtain a binary (i.e., cloud/no cloud) field with the specified cloud cover. This process defines the spatial distribution of cloud elements in the horizontal domain.

For cirriform and stratiform cloud types we build vertical structure around the cloud elements to produce visually realistic layer formations. We simulate the internal water density perturbation field using a four-dimensional version of the RSA model. We then convert the density perturbations to absolute liquid water content (LWC) using computed field statistics and a mean LWC profile generated following Ref. 4.

The cumuliform model is slightly different. We use a convection model based on the "parcel" method (Refs. 5, 6, and 7) to simulate cumulus formation and growth. In brief, we simulate cumulus as the sum of a large number of individual parcels. Each parcel is released from the lifting condensation level (as determined from a user-supplied meteorological sounding) with an initial upward momentum and size defined by the value of a random heating function. We then update the temperature, velocity, position, liquid water content, mixing ratio, etc. of each parcel at each model time step. The heating function is generated using the RSA fractional Brownian motion model. It may be desirable in the future to drive the cumulus convection model with a user-specified heating function which is correlated with terrain features such as cities, lakes and vegetation.

The temporal component of the enhanced cloud scene simulation model consists of two parts: advection and evolution. Advection is the process of shifting the cloud with the winds (obtained from the input sounding) and evolution involves modeling the fourth (temporal) dimension of the internal LWC perturbation field as fractal with specified temporal parameters. It is important to note that the advection/evolution model is intended for short temporal periods only (on the order of 5-15 minutes), and that the temporal model works only with the regular Cartesian output grid

4

1.3 ORGANIZATION OF THIS REPORT

This report, along with Ref. 1, documents the technical findings TASC has made during the SWOE cloud modeling effort. Section 2 describes the unique capabilities of the enhanced cloud model. First, we describe the variable-resolution output grid and compare it to the Cartesian grid. In Section 2.2 we detail the fractal algorithm that is used to generate the spatial distribution of cloud elements and their internal density structure. Section 2.3 focuses on the temporal component of the model. There we present a series of consecutive images that show the evolution of a cloud field over time. We end Section 2 with an outline of the cumulus convection model and a discussion of the fundamental equations (and their parameters) that drive the convection. We also include a few vis alizations of cumulus fields generated with the enhanced model.

Lastly, Section 3 contains a summary of the activities completed under the Cloud Scene Model Development Project. In that section we also outline recommendations for future additions and improvements to the cloud scene simulation model.

2. THE ENHANCED CLOUD MODEL

2.1 THE VARIABLE-RESOLUTION GRID

Requi   nents 6 and 7 listed in Table 1 refer to the size and resolution of the output cloud domain. In the enhanced model, we implemented a variable-resolution grid option to satisfy both the high resolutions and the large domain sizes required by the SWOE program. The variable-resolution grid allows the user to simulate higher resolution near the center of the cloud domain (the region of interest) and lower resolution toward the edge of the domain (the horizon) for the same computational cost and memory requirements as a medium-resolution standard Cartesian grid domain.

The variable-resolution grid is based on cylindrical coordinates (r, θ, z) where radial increments, Δr, need not be constant. Figure 1 shows horizontal slices through Cartesian and variable-resolution cylindrical grids side by side with approximately the same number of gridpoints in each. (A gridpoint is defined as the center of a grid volume.) The variable-resolution grid is defined by the inner and outer radial resolution (Δr_0 and Δr_{N-1},

Constant-Resolution Cartesian   Variable-Resolution Cylindrical
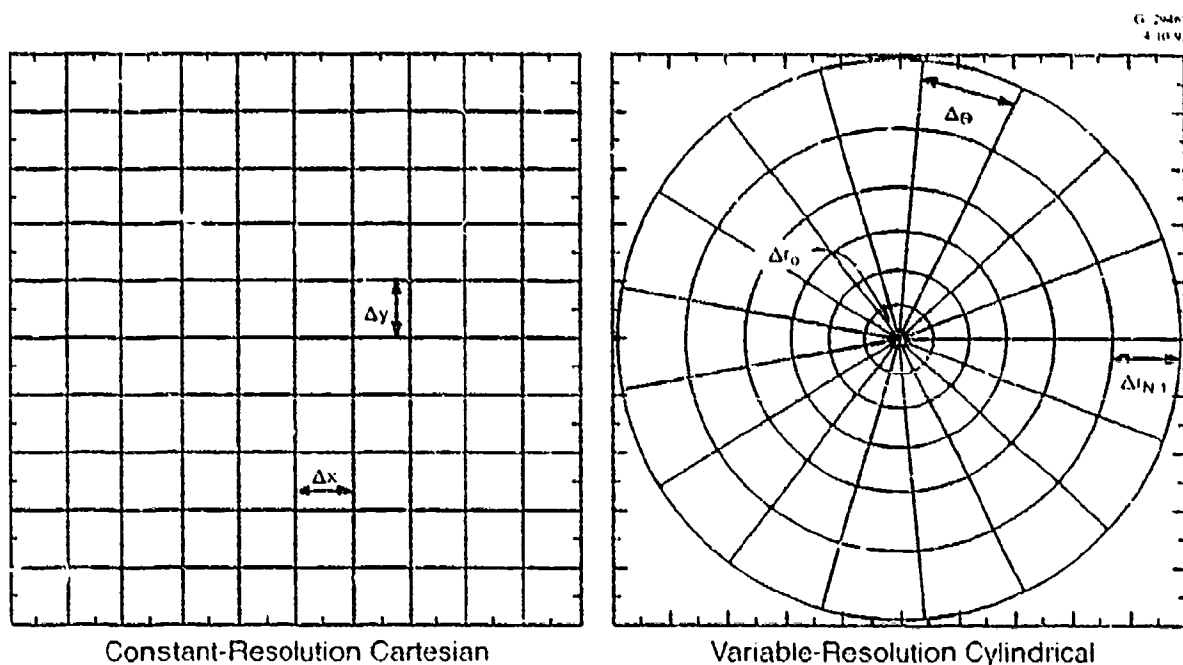
Figure 1   Comparison of a Horizontal Cross-Section Through
Cartesian and Cylindrical Output Grids

6

where N is the number of gridpoints in the radial direction), the angular resolution ($\Delta\theta$), the vertical resolution (Δz) and the radial extent of the model domain (R_{max}). All of these parameters are supplied by the cloud model user as described in Ref. 2.

When radial increments are constant, the horizontal area of a grid element increases linearly with distance r from the center of the grid as

$$\text{Area}_i = r_i \, \Delta\theta \, \Delta r \qquad (2.1\text{-}1)$$

where the subscript i is the grid element index along a radial line. For the variable-resolution cylindrical grid, radial increments vary from Δr_0 to Δr_{N-1} (corresponding to the center and the edge of the grid, respectively) by the following relationship

where

$$\Delta r_i = ai + b \qquad (2.1\text{-}2)$$

$$a = \frac{(\Delta r_{N-1} - \Delta r_0)}{(N-1)}$$

$$b = \Delta r_0.$$

The constant "a" is positive when the resolution is higher at the center of the grid, and negative when it is lower. For positive a, the grid element area for a variable-resolution grid increases faster than in Eq. 2.1-1.

The number of increments in the radial dimension, N, can be found by first summing over all the radial increments as follows:

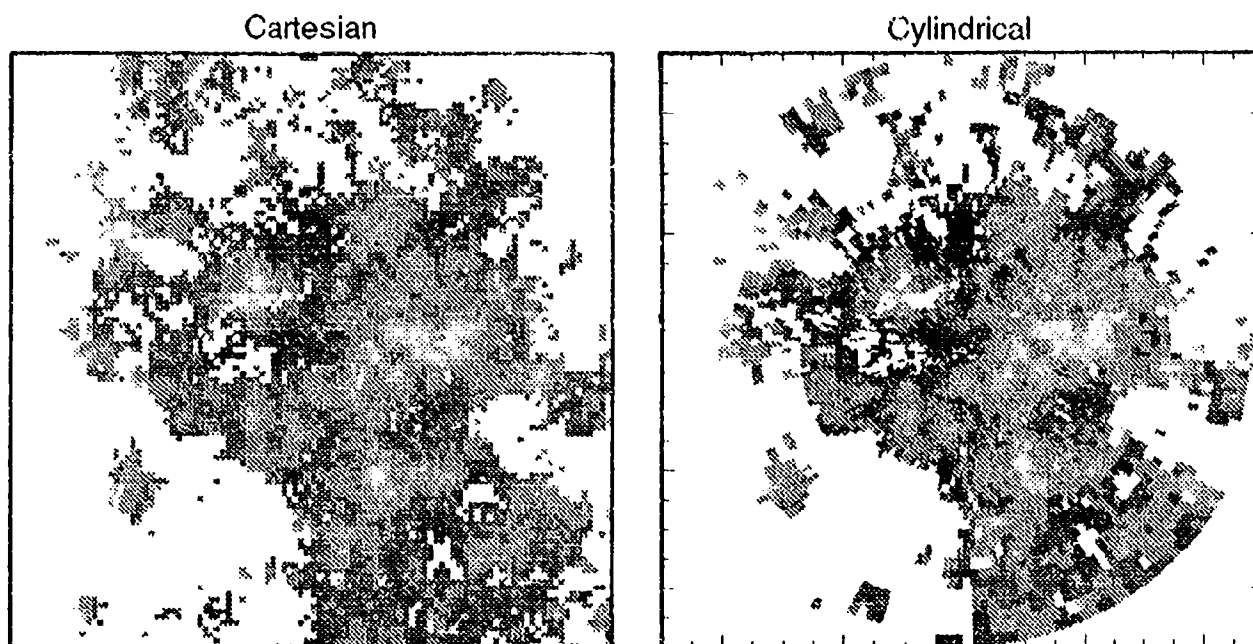$$R_{max} = \sum_{N-1}^{i=0} \Delta r_i \qquad (2.1\text{-}3)$$

using Eq. 2.1-2

$$R_{max} = a\frac{N\,(N-1)}{2} + b\,N \qquad (2.1\text{-}4)$$

and solving for N gives

$$N = \frac{2R_{max}}{(\Delta r_{N-1} + \Delta r_0)} . \qquad (2.1\text{-}5)$$

Figure 2 shows a two-dimensional slice through a model-generated cloud scene on both Cartesian and cylindrical output grids. All input parameters for the two realizations

7

Figure 2 Comparison of a Horizontal Cross-Section Through Identical
Cloud Fields Generated on Different Output Grids

are identical with the exception of the output grid option. Both realizations have the same number of gridpoints, but the cylindrical grid resolution is much higher at the center of the grid than the Cartesian.

The variable-resolution grid option is useful when higher resolution is required near the center. It provides the user with an extra degree of control of the size and resolution of the cloud model domain. As we will see in the next section, the extra flexibility available with the variable-resolution grid option necessitated a change in the fractal algorithm.

2.2 THE RESCALE AND ADD ALGORITHM

The successive random additions (SRA) fractal algorithm used in the interim model (and documented in Refs. 1 and 8) requires Cartesian grid geometry. It is one of a family of displacement techniques that approximates fractional Brownian motion in a region by iterative interpolation and addition of Gaussian noise over a larger region. With the addition of the variable-resolution capability in the enhanced model, we replaced the SRA technique with a more flexible algorithm; the rescale and add algorithm (Ref. 3).

8

The rescale and add (RSA) algorithm is rooted in the classical Weierstrass-Mandelbrot function which has been shown to approximate fractional Brownian motion (Ref. 9). Unlike the many displacement techniques, the RSA algorithm *does not* require a Cartesian output grid. The RSA method provides efficient point-wise evaluation of the fractal function directly on the output grid; there are no intermediate grids or results.

The RSA model approximates fractional Brownian motion in n dimensions as the sum of individual "frequencies" sampled from an n-dimensional lattice of random numbers. The lower frequencies provide large-scale structure in the field and the higher frequencies provide texture. Similar to the SRA algorithm, we control the character of the resulting field by varying a few key parameters.

The RSA model implementation consists of two steps. First, initialize an n-dimensional lattice with independent, zero-mean, normally distributed random values (we use unit variance, though it is not necessary). This lattice is relatively small (40×40×10×10 in the enhanced model) and is stored in computer memory. Second, following the RSA formula, sample the random lattice for each of the specified frequency terms and sum these terms to give the value of the function at any point on the output grid, V($\underline{x}$). The RSA formula i

$$V_n(\underline{x}) = \sum_{k=k_0}^{k_1} \frac{1}{r^{kH}} S_n[f(r^k\underline{x}')]$$
(2.2-1)

where

- n is the number of topological dimer⋯ (4 in our implementation)
- k_0 and k_1 are the lower and upper s⋯ation limits
- H is the Hurst parameter
- r is a lacunarity parameter
- $S_n[f(r^k\underline{x}')]$ is a smooth interp⋯ ⋯⋯ ⋯ m the random lattice to the position $r^k\underline{x}'$.

The lattice position, $\underline{x}'$, is relate⋯ ⋯⋯ ⋯put grid position, $\underline{x}$, by the resolution parameter which is not shown explicitly in the RSA formula.

For each term in the RSA sum, we evaluate the function $f(r^k\underline{x}')$ to determine the interpolation location. The value of the function consists of an integer part ($0 \leq d < N$) and a fractional part ($0 \leq \eta \leq 1$). The integer portion is computed using

$$d_i = \lfloor r^k x_i' \rfloor \text{ modulo } (N_i - 1), \quad i = 1, 2, ..., n$$
(2.2-2)

9

where N_i is the number of lattice gridpoints in the ith coordinate direction and "$\lfloor \ \rfloor$" computes the integer portion of a real number. As suggested by Saupe in Ref. 3, we use a cubic function to determine the fractional portion, η:

$$\eta_i = \Delta x_i^2 (3 - 2\Delta x_i), \qquad i=1,2,...,n. \qquad (2.2\text{-}3)$$

where

$$\Delta x_i = r^k x_i' - \lfloor r^k x_i' \rfloor, \qquad i=1,2,...,n \qquad (2.2\text{-}4)$$

As Saupe points out, the first derivative of the cubic function is continuous, unlike the standard linear weighting function. Although the cubic function slightly increases computational time to perform interpolations, it also reduces visible artifacts for a more realistic overall field.

The implementation of the RSA formula and a discussion of the model parameters follow immediately. Later in the section we describe the application of the RSA technique to the enhanced cloud model and show a few results.

Implementation and Model Parameters

There are five parameters in the RSA model that control the character of the final field. Four have been introduced directly with the RSA formula: the Hurst parameter, the lacunarity parameter and the upper and lower summation limits. The resolution of the lattice is the fifth parameter.
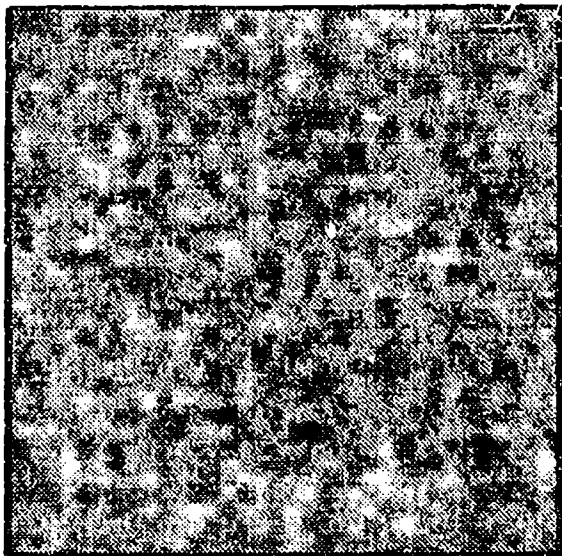
Lattice resolution — The resolution parameter relates the physical output grid to the random lattice. The lattice position ($\underline{x}'$) is computed from the output grid location ($\underline{x}$) as

$$x_i' = x_i / R_i, \qquad i=1,2,...,n \qquad (2.2\text{-}5)$$

where R_i is the lattice resolution in the ith coordinate direction. The resolution parameter specifies the number of output gridpoints per lattice point. Figure 3 shows the effect of varying resolution parameters. The intensity of the field values in each image is represented by a grey scale, where gridpoints with high numerical values are lighter, and darker gridpoints have lower values. Each output image is 350 by 350 pixels in size. The resolutions vary from 10 to 100 pixels/lattice point (where we use the same resolution parameter in both the x and y coordinate directions). It is clear from the figure that the resolution controls the spatial distribution of field values. The large-scale structure (due

10

Resolution = 10

Resolution = 25
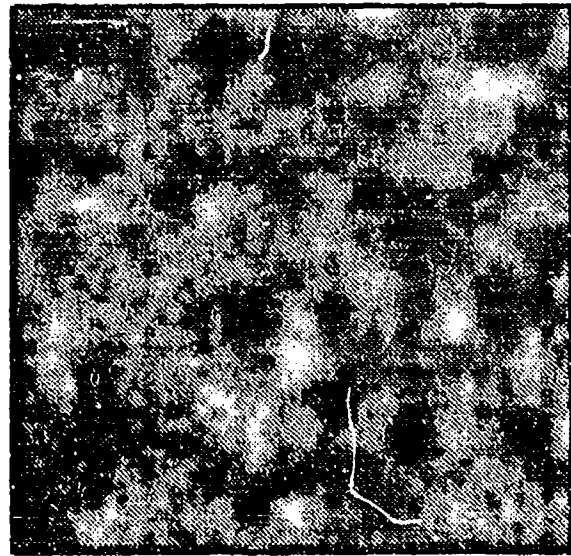
Resolution = 50

Resolution = 100

Figure 3   Series of Grey-Scale Images Showing the Effects of Varying
the Lattice Resolution in the RSA Model

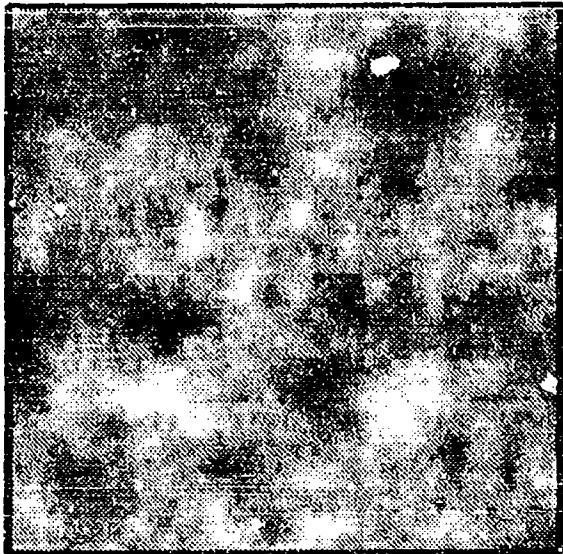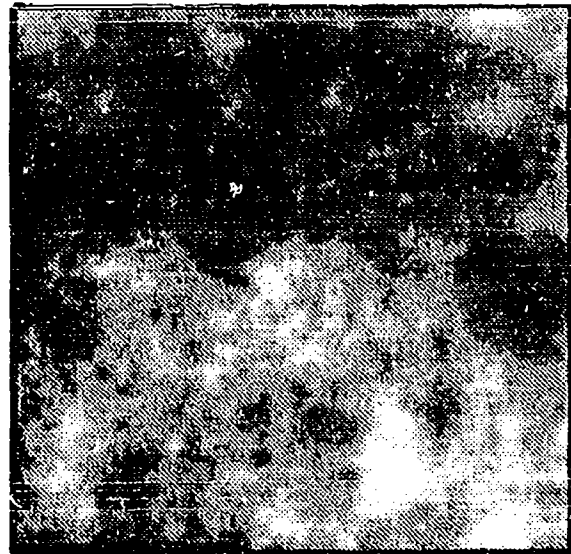to the zeroth frequency band in the RSA formula) in the first image (resolution = 10 points/lattice point) is based on the first 36 by 36 gridpoints in the random lattice. The zeroth frequency band in the last image (resolution = 100) uses only the first 5 by 5 lattice points, resulting in much smoother spatial distribution. The qualitative effect of varying the resolution parameter in the RSA is akin to varying the lacunarity parameter in the SRA algorithm (Ref. 1).

Summation Limits — The summation limits k_0 and k_1 in the RSA formula are chosen to represent all spatial scales of the desired output field (Ref. 3). Saupe discusses selecting a value for the lower limit, k_0, to represent the largest spatial scale in the output field, and the upper limit, k_1, the smallest scale.

For our cloud model application (and corresponding spatial scales), we found that negative terms add almost undetectable variations to the final field. By setting $k_0 = 0$, we achieve large-scale sizes (on the order of the resolution parameter) without the computational cost of adding negative terms. The upper summation limit is chosen in order to enable us to differentiate between adjacent gridpoints in the final field. Using $k_1 = 4$ enables us to differentiate grid points separated by as little as 10 meters for the lacunarity parameter and lattice resolution used in the model. The highest frequency data are smoothly interpolated to resolutions beyond 10 meters. For applications requiring higher resolution, the upper summation limit should be increased accordingly.

Figure 4 contains images of five individual frequency terms: $k = 0, 1, 2, 3, 4$. The lower right image in the figure is the RSA fractal field produced by summing the 5 terms according to Eq. 2.2-1. Each image is scaled to fill the range of 256 grey-scale colors for visualization. The figure shows that each successive frequency band reaches farther into the random lattice as prescribed by the $r^k \underline{x}'$ term in Eq. 2.2-1.

Lacunarity Parameter — The lacunarity parameter in the RSA model controls different field characteristics than the lacunarity parameter previously described in Ref. 1 and used in the SRA algorithm. Its effects on the final fractal function are bound together tightly with the choices of resolution parameters and summation limits, and thus are slightly more difficult to detect.

The lacunarity parameter, r, is used in two distinct places in the RSA formula. First, r^k multiplies $\underline{x}'$ to determine the location to interpolate from the random lattice. For
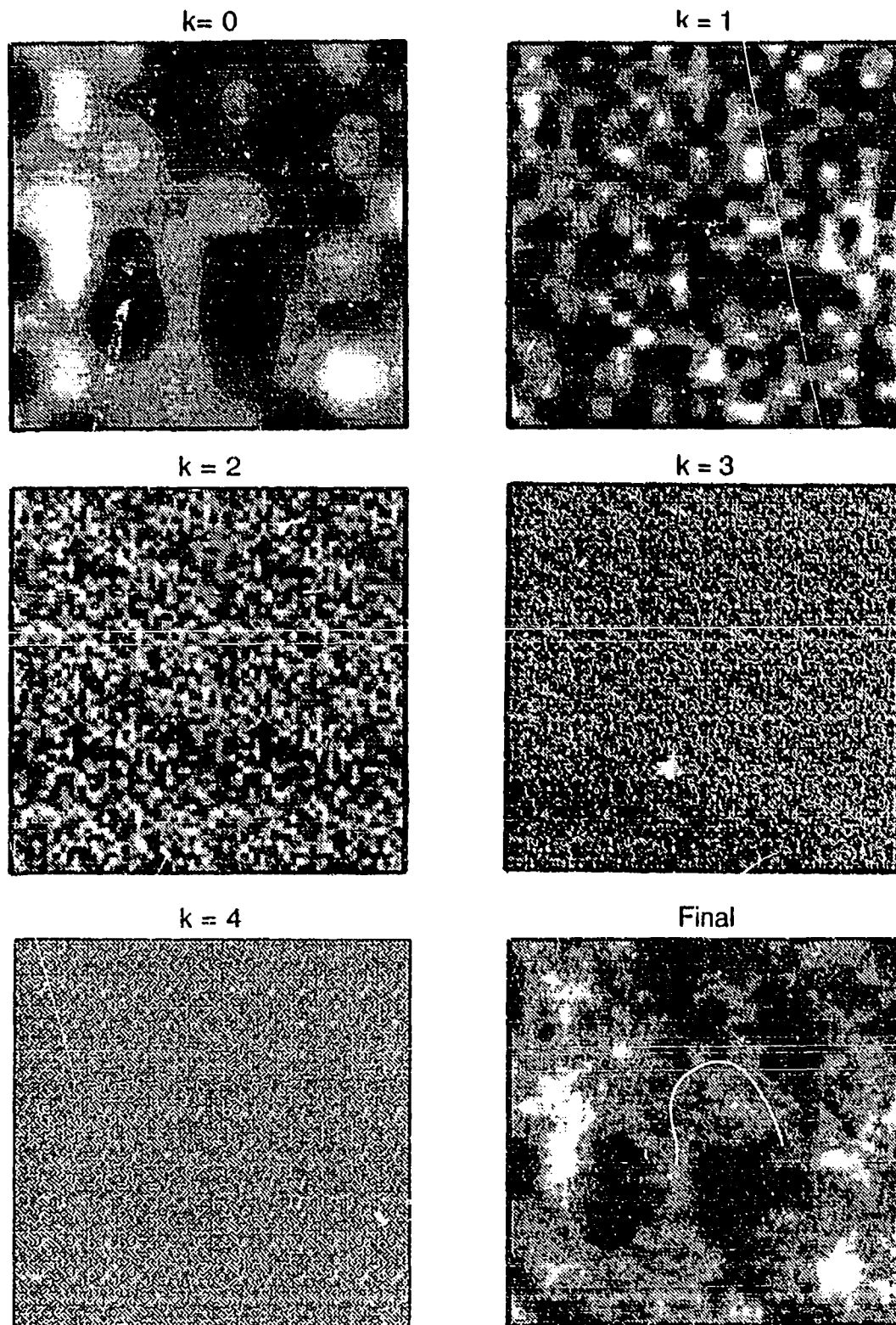
Figure 4   Grey-Scale Images Showing Five Frequency Terms and the Resulting RSA Field Generated by Summing the Terms

13

constant k, larger r values correspond to larger increments between evaluation points in the random lattice and greater variability in the texture of the final field. Smaller r values correspond to finer increments and overall less variability.

The second use for the lacunarity parameter is in the amplitude term in Eq. 2.2-1; $1/r^{kH}$. The amplitude multiplies each frequency term, producing decreasing amplitudes for increasing frequency. For constant Hurst parameter, consecutive terms drop off more (less) quickly for higher (lower) lacunarity parameter values.

These two effects act in concert to produce fields that vary from being smooth with little small-scale structure (low r) to rough with greater small-scale detail (high r). Though Saupe doesn't mention explicit limits on the value of r, we found in practice that scenes generated with lacunarity parameters greater than 5 were almost indistinguishable from scenes with r=5. This is due to the rapid drop in amplitude of the higher frequencies. In Figure 5 we include four grey scale images with values for the lacunarity parameter varying from 2 to 5. We found a practical lower limit of r=2 through experimentation and familiarity with the RSA algorithm. Smaller lacunarity values can be used if k_1 is increased accordingly.
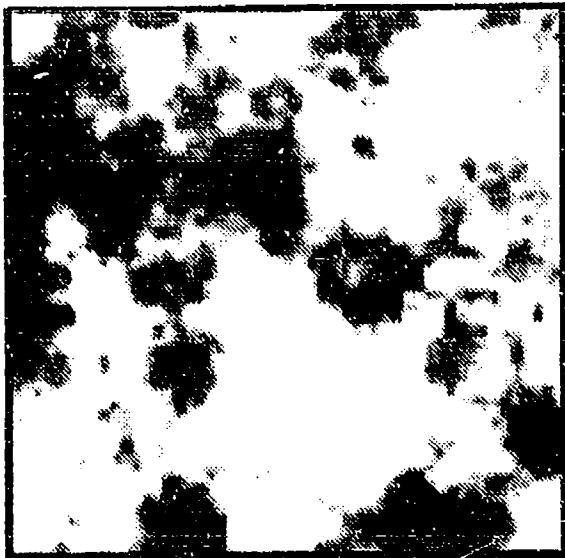
Hurst Parameter — Like the lacunarity parameter, the Hurst parameter also controls the amplitude of each term in the RSA sum. However, its effects on the final field are much easier to detect. Mathematically, higher H values cause the amplitude term in Eq. 2.2-1 to decrease more rapidly with increasing frequency index, k. In an opposite way, lower H values imply a more slowly decreasing amplitude term (and thus greater influence of high frequency terms). The qualitative effects can be seen in Fig. 6 where each image grows smoother with increasing H. We see that the qualitative effects of variations in H are almost identical to the SRA algorithm; the large-scale structure remains invariant with different H values, but the small-scale variability (i.e., the roughness) of the field changes.

Application of the RSA Algorithm to the Enhanced Cloud Model

The rescale and add algorithm is used for five distinct purposes in the cloud model. It is used to:

- Generate the 2-d horizontal distribution of cloud elements in each layer
- Determine the height of the cloud top at each gridpoint

r = 2   r = 3
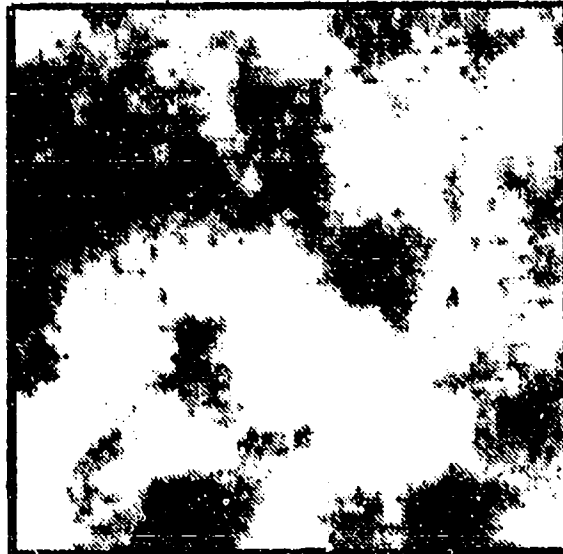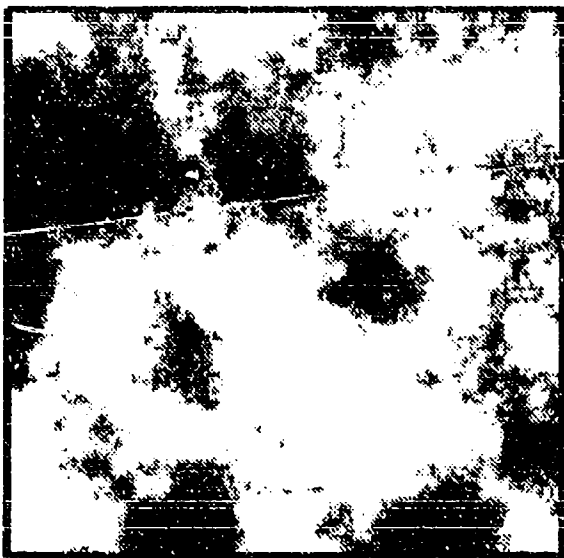
r = 4   r = 5
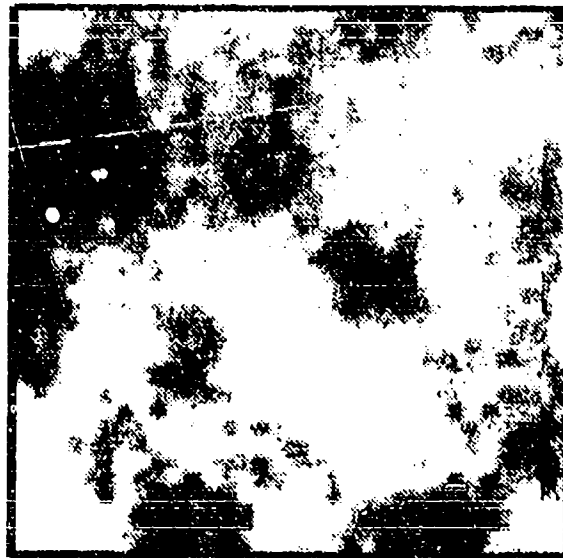
Figure 5   Sequence of Grey-Scale Images Generated With the RSA
Model with Various Values for the Lacunarity Parameter

15
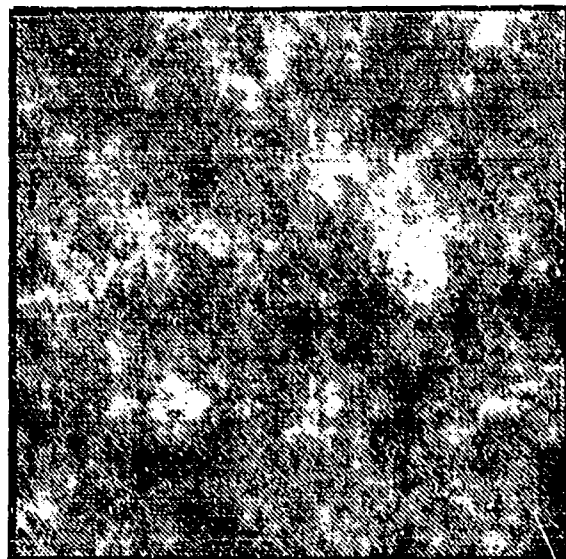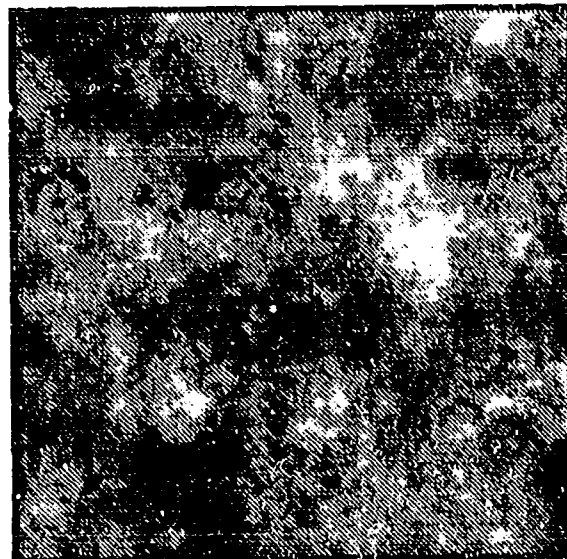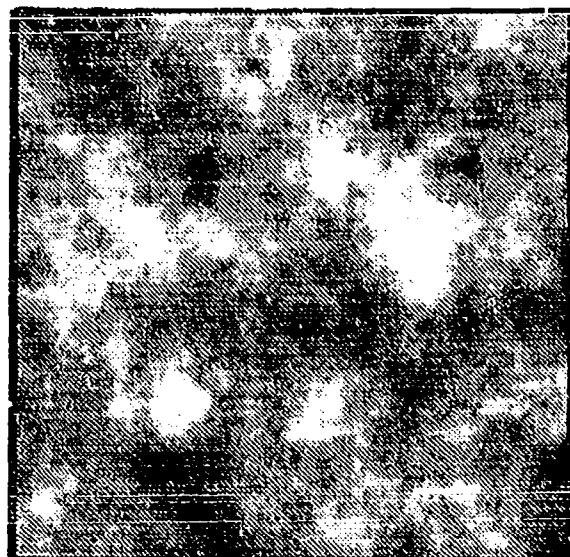
H = 0.2   H = 0.4   H = 0.6   H = 0.8
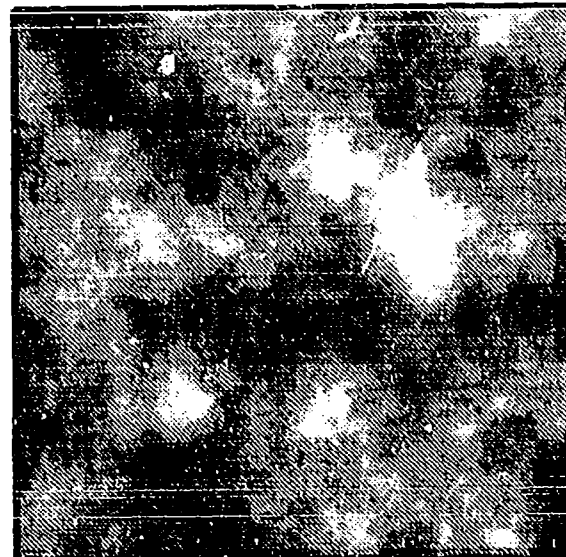
Figure 6   Sequence of Grey-Scale Images Generated With the RSA
Model with Various Values for the Hurst Parameter

- Simulate variability in the cloud base surface
- Generate the internal water density perturbation field in 4-d
- Define the random heating function to drive cumulus convection.

The first four functions are used to model stratiform and cirriform cloud types. They are the subject of the remainder of this section. The fifth function is unique to the cumulus model. It is discussed further in Section 2.4.

To begin the enhanced cloud model, we initialize a four-dimensional random lattice. The four dimensions correspond to the x, y, z and time dimensions. All RSA model computations reference values from this one lattice.

Applying our knowledge of the RSA algorithm and the structure and variability of cloud fields of different types, we selected values for the five model parameters for each cloud type. With regard to summation limits (discussed above), we use $k_0 = 0$, $k_1 = 4$ in all of the RSA functions and for all cloud types. Similarly, we use only one lacunarity parameter value ($r = 3$) for all functions and cloud types. The remaining parameters: the Hurst parameter and lattice resolution provide enough flexibility to simulate fields of widely varying characteristics, including non-isotropic cirriform cloud fields.

The lattice resolution controls the spatial scale of the model field. For example, larger resolutions produce cloud/no cloud elements for the horizontal cloud field. Smaller lattice resolutions are used to produce variability along the cloud base surface. Even smaller resolutions are used to simulate the highly variable distribution of LWC within cloud elements. Similarly, the Hurst parameter varies with cloud type and usage. We defined H values for cloud/no cloud field generation based on empirical data f scientific literature (Refs. 10 and 11) and visual appearance. Hurst param... values in the simulation of the LWC perturbation field are based on our previous analys. o aircraft LWC measurements (see Ref. 1) as well as visual appearance.

Figure 7 shows sample horizontal slices through 3-d cloud fields generated with the enhanced cloud model of three cloud types: stratus, stratocumulus and cirrus. Each figure represents an area 20 km × 20 km in size, where black areas correspond to no cloud and a grey scale is used to show the internal density field within cloud regions. The Hurst parameter and lattice resolution values used to generate cloud/no cloud structure within the scenes are contained in Table 2. Notice that we use anisotropic lattice resolution to

17

Stratus

Stratocumulus
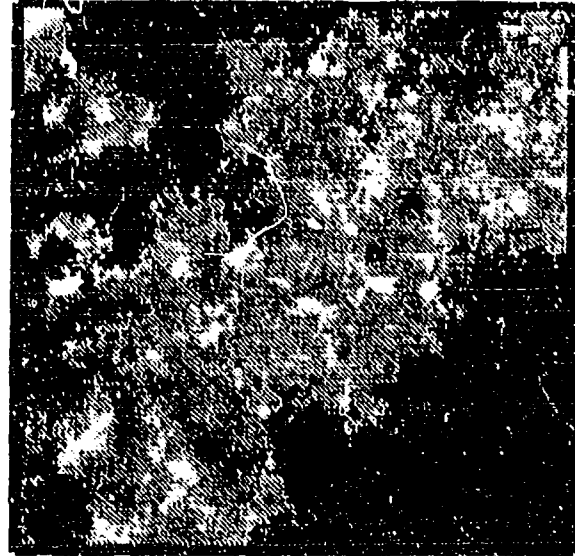
Cirrus
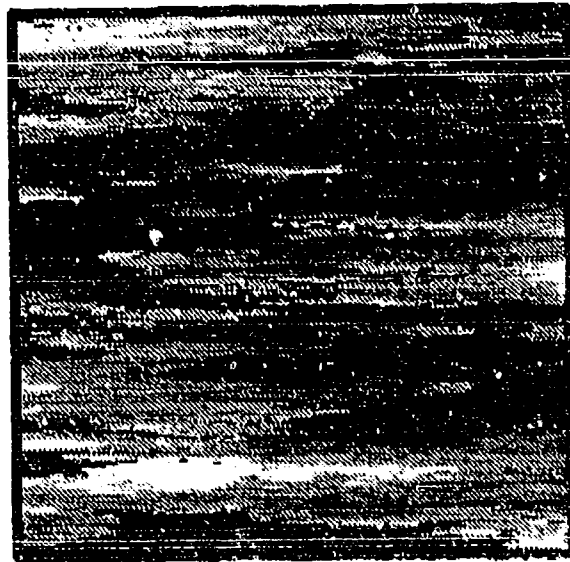
Figure 7   A Horizontal Slice Through Cloud Scenes of Various Types
Generated with the RSA Model (All Have 60% Cloud Cover)

18

Table 2   Default Values for the Hurst Parameter and Lattice Resolutions Used in the Generation of the Horizontal Cloud/No Cloud Field for Various Cloud Types

	H	R_x (km)	R_y (km)
Stratus	0.7	30	30
Stratocumulus	0.3	6	6
Cirrus	0.4	20	2

simulate the banded/fibrous nature of cirrus. (Recall in the interim model we used anisotropic lacunarity parameters for the same effect.) Different parameters are used to simulate the internal density field.

Results

The SRA algorithm, used in previous versions of the cloud model, was replaced to enable point-wise evaluation of a fractal field (needed for the variable-resolution output grid). Based on our experience with several fractional Brownian motion models, we chose the RSA for its mathematical soundness and its flexibility. We have shown two-dimensional views of the model output data. In Figs. 8 through 10 we show three-dimensional views of the same three cloud types. All are single layer cloud scenes with 60% fractional coverage extending over an 10 km x 10 km domain. We display the scenes as viewed from above and off to the side (similar to the view from an airplane window) to show not only the horizontal distribution of cloud elements, but also their vertical variability.
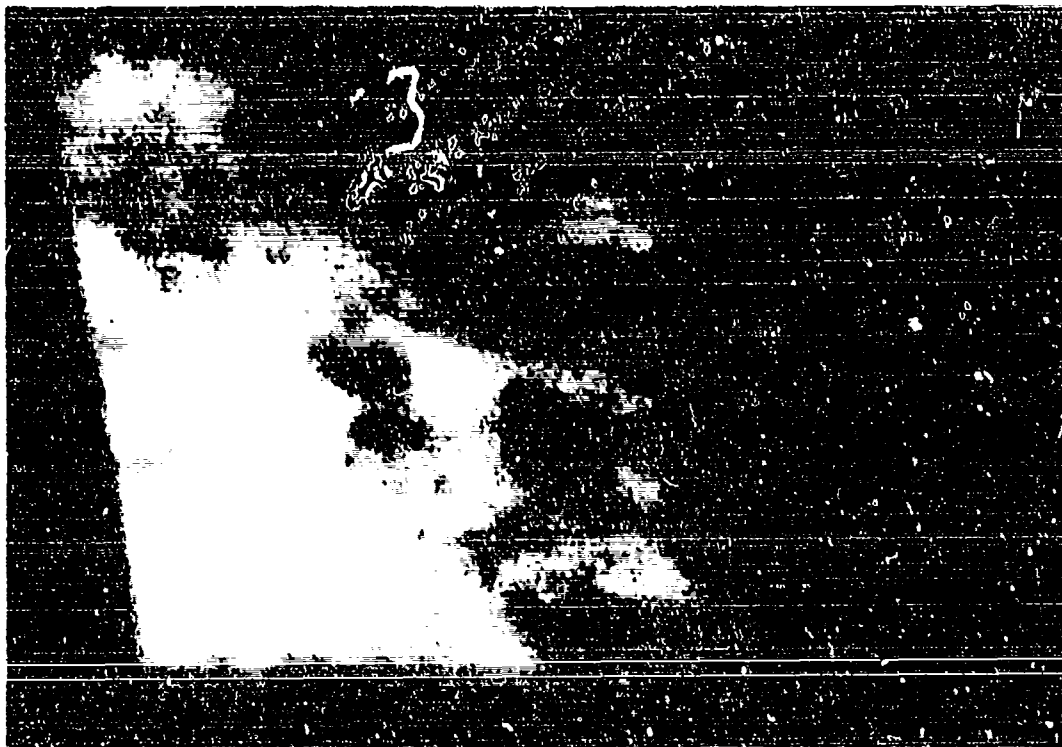
Figure 8   Stratus Cloud Layer Produced with the Enhanced Cloud Model (60% Cloud Cover, 10 × 10 km Horizontal Extent)

Figure 9   Stratocumulus Cloud Layer Produced with the Enhanced
Cloud Model (60% Cloud Cover, 10 × 10 km Horizontal Extent)

Figure 10   Cirrus Cloud Layer Produced with the Enhanced Cloud
Model (60% Cloud Cover, 10 × 10 km Horizontal Extent)

2.3 TEMPORAL EVOLUTION

A requirement of the SWOE program is to model not only the spatial variability of cloud fields, but also their temporal variability over short time periods (approximately 5-15 minutes). We model two temporal processes for cirriform and stratiform cloud types: horizontal advection due to local winds and stochastic evolution that describes the growth, change and decay of cloud elements. The temporal evolution of cumulus is described in Section 2.4.

We begin this section by describing both the advection and evolution components of the model. We then present a few temporal sequences with varying parameters and discuss the selection of those parameters.

Advection — The cloud model user provides historical weather data by means of a sounding. The sounding meridional and zonal wind components drive the temporal advection. We assume constant wind speed and direction over the model period and horizontal domain. In general, the model domain is larger than the output grid domain to accommodate the movement of clouds across the scene. The size of the domain is determined by the maximum wind acting over the entire time period.

We use the RSA model to generate the horizontal distribution of cloud elements over the entire scene as described previously. Upper and lower cloud surfaces are built around each cloud element. The initial (time=0) field is independent of the wind. Each successive output scene advects and evolves from the previous field. Winds are linearly interpolated from the sounding data to each vertical level of the cloud scene.

Each level within the cloud domain is advected based on the winds at that level. Advection affects both the outer cloud surfaces and the interior gridpoints. Figure 11 shows a schematic of a cloud surface before and after advection. The figure also shows the relative wind vectors used to advect the surface. This process allows for wind shear within a cloud layer as well as shear between layers.

Evolution — Advection simply moves the cloud field. We also use the four-dimensional RSA to *evolve* the field. The density at every interior cloud voxel is determined using the RSA formula and the 4-d random lattice. The x-y-z position of each voxel (used to compute a position within the random lattice) takes into account shifts due to

23
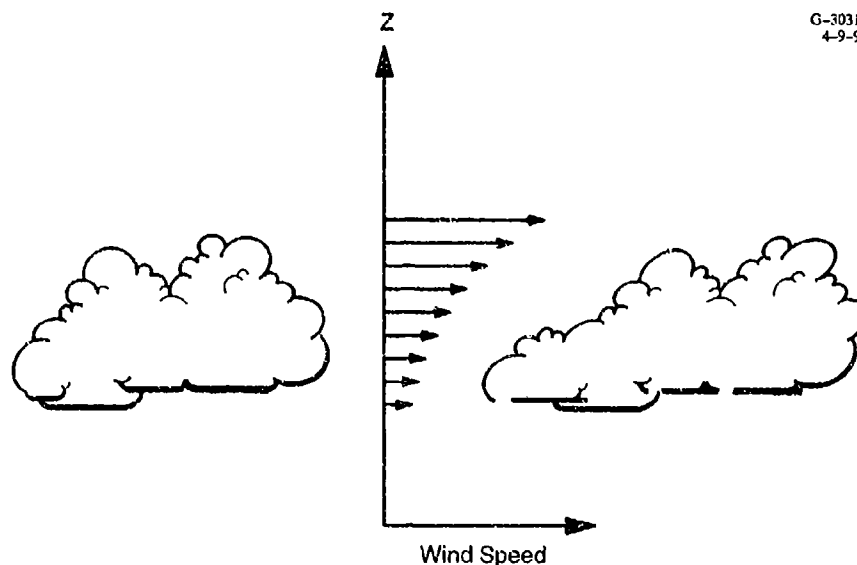
Figure 11   Schematic Showing the Effects of Wind Shear
Within a Cloud Layer

advection. Time is specified by the number of seconds since initialization. The resolution of the random lattice in the time coordinate is the key parameter that controls the rate of evolution within the cloud model. A short temporal resolution implies a rapid rate of evolution and a longer resolution implies slower change.

Results — Figures 12 and 13 present sequences of cloud scenes, one scene every 30 seconds for 4.5 minutes. Each figure shows a horizontal slice through a cloud LWC field (10 km on a side) as it changes over the period. LWC values are shown in color against a blue background. Light grey regions represent low LWC increasing toward yellow and orange. The areas of highest LWC are colored red. Figure 12 used a temporal lattice resolution of 2 minutes, Figure 13 used a lattice resolution of 5 minutes. Qualitative comparison of the two sequences shows that the rate of change in the first sequence is indeed faster than in the second. As with the spatial resolution parameters, we define the temporal lattice resolution as a function of cloud type. We choose a 5 minute resolution for stratus and altostratus cloud types and 2 minute for stratocumulus and altocumulus and cirriform cloud types. The choices of temporal resolution in the enhanced model are based only on qualitative comparison of different cloud fields and are not based on any physical cloud data. Ideally, we would base parameter selection on analysis of observed cloud LWC data.
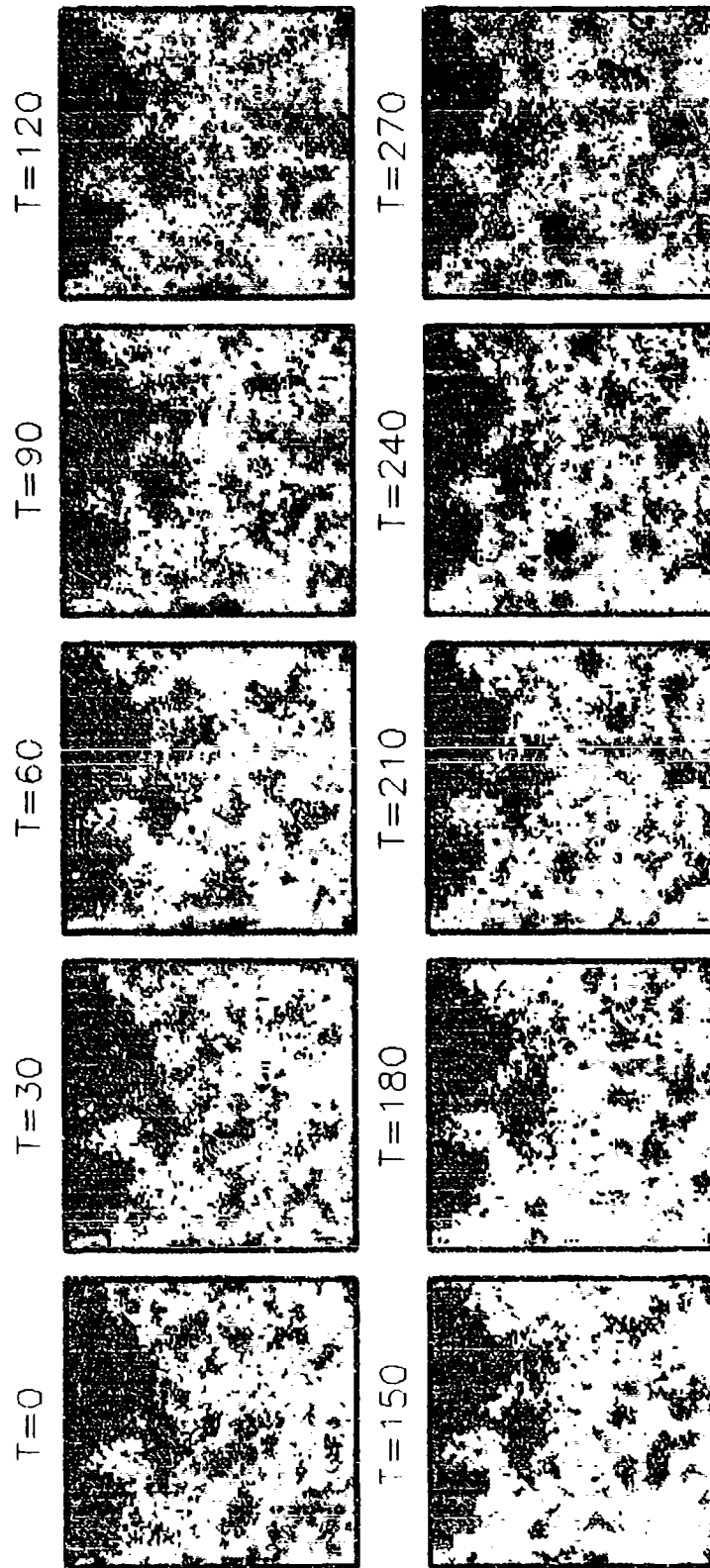
Figure 12   Sequence Showing Cloud Field Evolution Every 30 Seconds for a 5 Minute Time Period (Temporal Lattice Resolution = 2 Minutes). Areas of High Density are Highlighted in Red
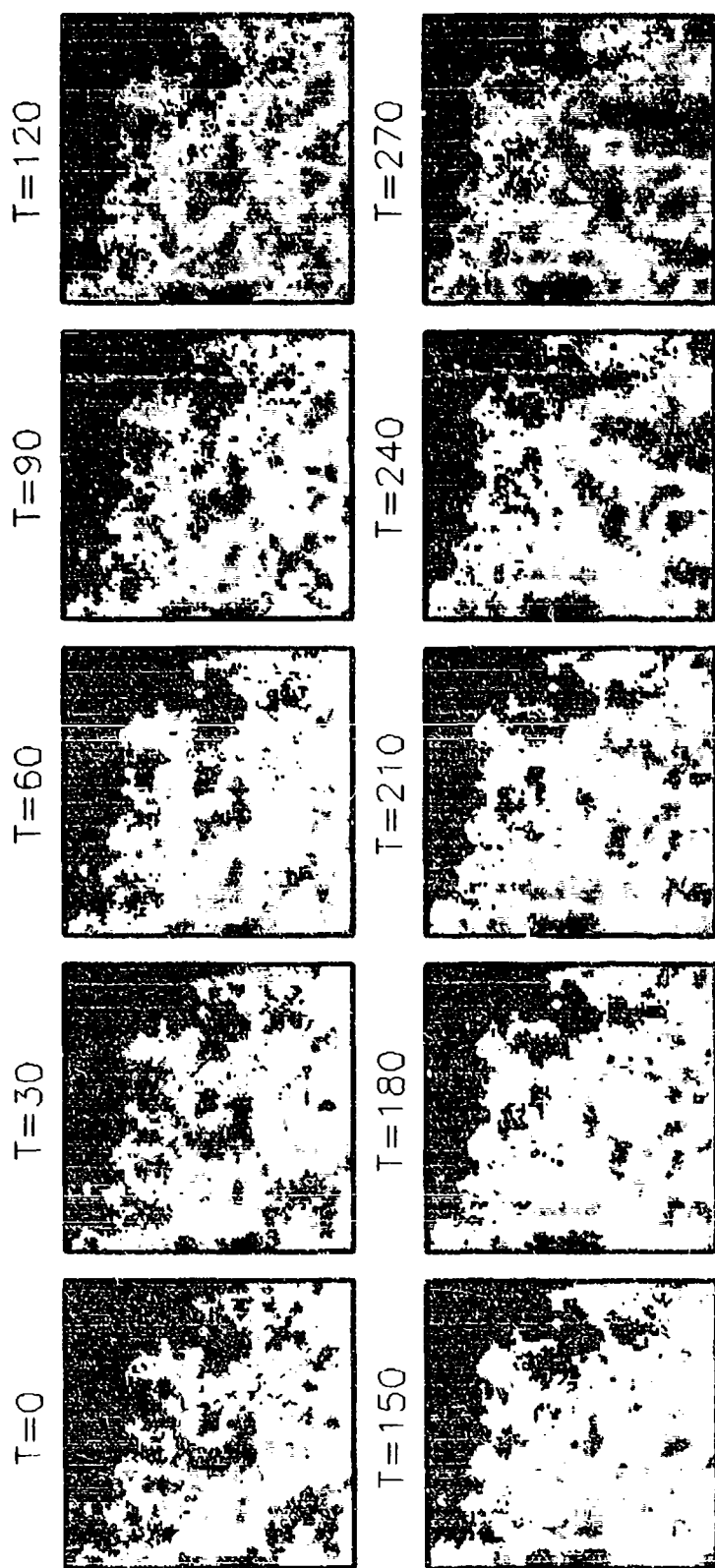
Figure 13   Sequence Showing Cloud Field Evolution Every 30 Seconds for a
5 Minute Time Period (Temporal Lattice Resolution = 5 Minutes).
Areas of High Density are Highlighted in Red

2.4   THE CUMULUS MODEL

Many models of varying complexity have been developed to simulate cumulus convection. They range from simple bubble convection models (Ref. 12) to 3-d models that simulate the complex dynamical and microphysical processes of cumulus clouds (Ref. 13). Due to the computer requirements of the SWOE program, we developed a relatively simple and efficient Lagrangian cumulus model based on the "parcel" method which simulates fair-weather (non-precipitating) cumulus cloud fields as the sum of many (approximately 1000) parcels of varying size and water density. Model-produced cumulus clouds form in an atmosphere described by a user-specified meteorological sounding containing temperature, moisture and wind information.

The model contains a few key parameters (e.g., maximum perturbation temperature, maximum parcel size, number of parcels, etc.) that are described later in this section. Throughout development we have tried to choose parameter values that produce the most realistic results. With continued use by other SWOE participants and testing of the cumulus model with a wider variety of environmental input data, we expect that some parameter values may change. We designed the model to make such changes relatively painless.

Parcel convection is driven by a slowly varying heating function (a function of both space and time) much like the time varying surface heating function discussed in Hill (Ref. 14). However, in the enhanced model, we use the RSA algorithm to simulate heating. The heating function is initialized from the same random reference lattice that is used elsewhere in the model. Convection is initiated at the lifting condensation level (LCL) computed from the user-specified input sounding. The LCL is the level at which parcels lifted adiabatically from the surface become saturated (i.e., the level at which the dry adiabat and the mixing ratio line defined at the surface intersect). We use the RSA algorithm to define a 3-d (space and time) perturbation temperature field at the LCL, where perturbation is defined with respect to the ambient temperature at that level. We apply a threshold to the RSA field that results in the desired cloud cover fraction. Values above the threshold are linearly transformed to perturbation temperature, where the minimum perturbation is 0.0 K and the maximum is 1.0 K. We show the effects of varying the perturbation temperature later in this section.

The RSA fractal model generates spatially correlated random fields with regions of high perturbation temperatures ("hot spots") and low perturbations. We expect greater

convection (corresponding to higher cumulus towers) at the "hot spots" in the model domain. The variability in the heating function and the spatial distribution of the "hot spots" is controlled by the same parameters discussed in Section 2.2, the Hurst parameter and the lattice resolution.

Parcels are released from random locations across that portion of the model domain with perturbation temperatures greater than zero. Parcel size is a linear function of the perturbation temperature, where the minimum size is the minimum resolution of the output domain and the maximum size is set to 1000 meters. For small output domains (less than 10×10 km horizontal extent), a smaller maximum parcel size may be required.

The driving force acting on the parcels is the buoyant force. It is derived from the hydrostatic equation using basic thermodynamic principles. The hydrostatic equation describes the change in atmospheric pressure as a function of height. It is

$$\frac{\delta p}{\delta z} = - \varrho g \qquad (2.4\text{-}1)$$

where δp is the vertical pressure change across a unit volume of air, δz is the change in height across the volume, ϱ is the density of the air and g is the gravitational acceleration. The buoyant force per unit volume on a parcel of density ϱ_p in an environment of density ϱ_a is written

$$F = (\varrho_a - \varrho_p)g. \qquad (2.4\text{-}2)$$

where we use the subscripts "p" to denote parcel and "a" to denote ambient conditions. Using Newton's second law and the equation of state for an ideal gas, we can solve for the vertical acceleration of a parcel in terms of its temperature. The vertical acceleration is given by

$$a = g\frac{(Tv_p - Tv_a)}{Tv_a} . \qquad (2.4\text{-}3)$$

It is important to use virtual temperature, Tv, in Equation 2.4-3 to account for the variation in density due to humidity. Virtual temperature is given by

$$Tv \approx (1 + 0.61 \ w) \ T \qquad (2.4\text{-}4)$$

where w is the mixing ratio (kg water vapor / kg dry air). The approximation is due to the fact that we use mixing ratio instead of specific humidity as a measure of water vapor content. The mixing ratio is a function of vapor pressure, e (in millibars),

$$w = 0.622 \times \frac{e}{(p - e)} \qquad (2.4\text{-}5)$$

where 0.622 is the ratio of molecular weight of water to dry air. For a saturated parcel, the vapor pressure is found (Ref. 15) using

$$e = e_0 \exp^{[17.67 \times T/(T + 243.5)]} \qquad (2.4\text{-}6)$$

where e_0 is the saturation vapor pressure of liquid water at 0.0 °C, and T is in °C. To find the vapor pressure of an unsaturated parcel, replace temperature in Eq. 2.4-6 with dewpoint temperature.

The model uses the equations above, along with many other supporting relationships, to solve for the position and state (i e., mixing ratio, temperature, etc.) of each parcel as a function of time. Parcels are initially released with upward velocity equal to zero. (A non-zero initial velocity may be more appropriate, though we did not simulate that aspect of parcel heating in this version of the cumulus model.) The model solves Eq. 2.4-3 exactly for the acceleration of the parcel (and thus the position) at each time step. Parcel temperature is updated by solving for the wet or dry adiabatic lapse rates depending on whether the parcel is saturated or unsaturated, respectively. The dry adiabatic lapse rate is

$$\Gamma_{dry} \equiv -\left(\frac{dT}{dZ}\right)_{unsat} = \frac{g}{c_p} \qquad (2.4\text{-}7)$$

where g, the gravitational acceleration, is a function of height, and c_p is the specific heat at constant pressure. This equation assumes that there is no heat transfer between the parcel and the surrounding environment and that the parcel is in equilibrium with its surroundings (i.e., $p_p = p_a$).

The saturated adiabatic lapse rate accounts for the release of latent heat which accompanies condensation as the saturated parcel rises through the atmosphere. (Likewise, absorption of latent heat during evaporation on descent.) The saturation lapse rate can be

29

found (approximately, see Ref. 6) as a function of temperature and saturation mixing ratio, w_s, from the following

$$\Gamma_{wet} \equiv -\left(\frac{dT}{dZ}\right)_{sat} \approx \frac{g}{c_p}\left[1 + \frac{Lw_s}{R_{ma}T}\right]\left[1 + \frac{L^2w_s}{c_pR_{mw}T^2}\right]^{-1} \qquad (2.4\text{-}8)$$

where

- L is the latent heat of vaporization (a slowly varying function of temperature)
- R_{ma} is the specific gas constant for dry air
- R_{mw} is the specific gas constant for water vapor.

The ambient temperature and dewpoint temperature, mixing ratio, etc. are also updated at each time step. Ambient temperatures are interpolated directly from the input sounding.

Up to this point we have not considered the effects of mixing with the environment on parcel convection. Mixing with the cooler, drier environmental air reduces the parcel buoyancy and the maximum cloud top height. The temperature of the parcel after entrainment, T_p', is the weighted average of the parcel and ambient air temperatures, T_p and T_a, respectively. If the mass of the parcel is denoted m_p and m_a is the mass of air entrained, T_p' is

$$T_p' = \frac{(m_pT_p + m_aT_a)}{(m_p + m_a)} \qquad (2.4\text{-}9)$$

Likewise, the mixing ratio after entrainment, w_p', is the weighted average of the mixing ratio of the parcel and the ambient air

$$w_p' = \frac{(m_pw_p + m_aw_a)}{(m_p + m_a)} \qquad (2.4\text{-}10)$$

As the parcel "dries out" by entrainment, more water must evaporate to keep the parcel saturated. The evaporation serves to cool the parcel even further through absorption of latent heat. Thus entrainment has a double effect on decreasing the temperature (and the buoyancy) of a parcel: first, the parcel cools due to mixing with cooler air and second, the parcel cools due to resaturation.

The mass of air entrained over any time period can be calculated by assuming a constant entrainment rate, E. E is given in terms of % mass increase per 100 mb.

Following Ref. 16, we use a value of 100%/100mb. That is, a parcel will entrain its entire mass over a 100 mb ascent (or descent).

The mixing process that takes place in cumulus growth is complex and not well known. In general, greater entrainment occurs near cloud edges and less in the interior of the cloud where the air is shielded from the environment. It is also true that the rate of entrainment changes with time in the cumulus cycle. Neither of these effects are currently accounted for in the mixing portion of the cloud model.

Results and Sensitivity Tests — In this section we include graphs that trace the vertical position of individual parcels as a function of initial perturbation temperature and entrainment rate. Saturated parcels originate at the LCL and rise through the atmosphere following a moist adiabat (modified by entrainment) until they cool below the ambient temperature. At that point, the parcels are negatively buoyant and fall back through the atmosphere warming as they fall and becoming unsaturated. Parcels are traced as they rise and fall repeatedly. A parcel becomes "inactive" once it hits the ground and another is released from the LCL to replace it.

Figure 14 shows 4 parcel paths (vertical motion only) where each parcel has a different initial perturbation temperature. We can see that the parcel with the highest temperature reaches the highest altitude. Not only does it have the highest apex, but it also reaches its apex quicker than the others. The damping of the vertical motion over time is due to entrainment.

The second figure (Fig. 15) shows three parcels with equal initial perturbation temperature (0.5 K), but differing entrainment rates. The entrainment rates vary from 50% to 200% mass increase per 100 mb. As one would suspect, the higher entrainment rates lead to greater damping and lower overall cloud top height.

At any time a snapshot of the cloud field reveals parcels at various points along their paths. The 3-d output field is generated by stepping through the output grid, identifying all parcels that overlap each gridpoint. A parcel overlaps a gridpoint if the magnitude of the three-dimensional vector from the center of the grid volume to the x-y-z center of the parcel is less than or equal to the size of the parcel (recall that parcel size is a function of the initial perturbation temperature). The sum of all the parcels produces a density field. We convert the density field to LWC following Feddes' method (Ref. 4) as with the cirriform and stratiform cloud types.
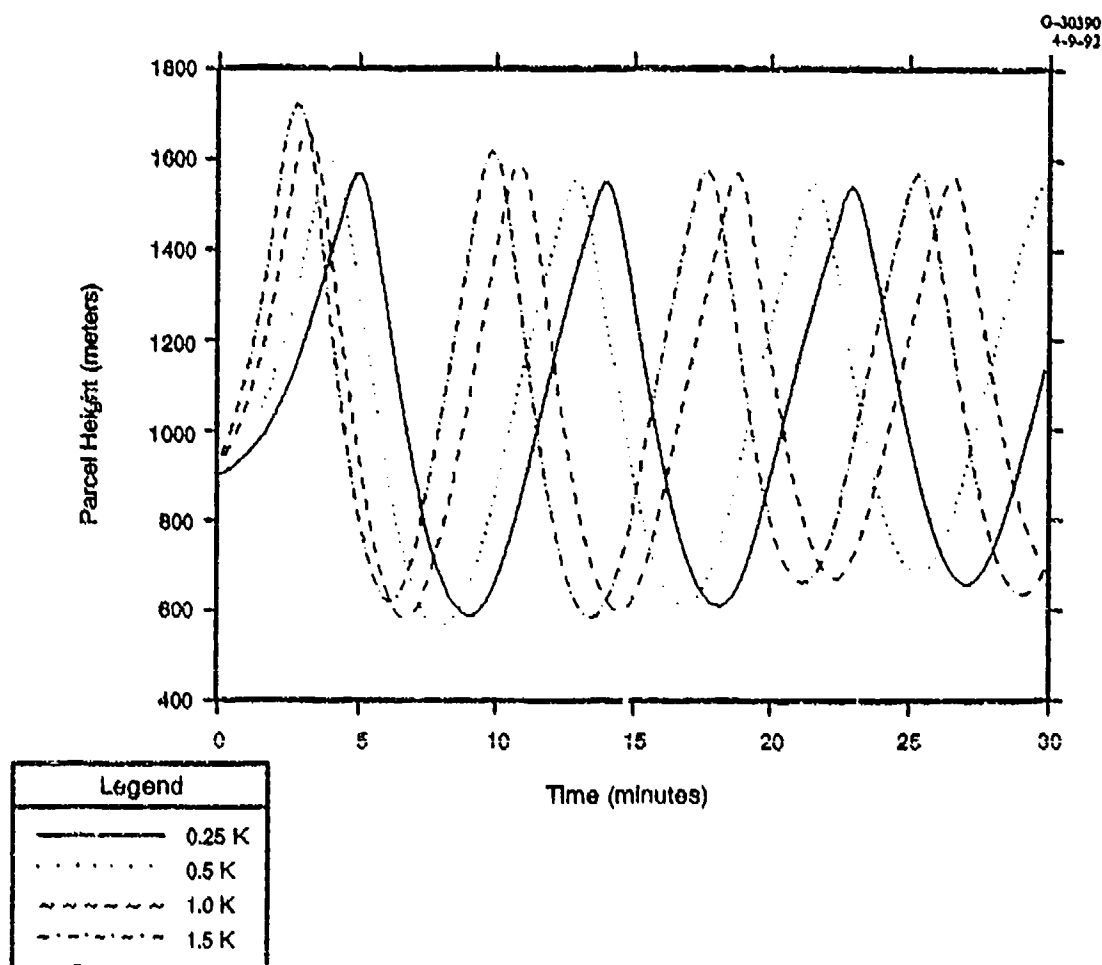
Figure 14   Vertical Position as a Function of Time for 4 Parcels with
Different Initial Perturbation Temperatures

Figures 16 and 17 show one cumulus cloud layer at two separate times. The first figure corresponds to the initial (time = 0) field. Just as in the cirriform and stratiform model, it does not contain the effects of horizontal wind advection. Figure 17 shows the same cloud field 3 minutes later (and includes advection effects). Horizontal winds alone, interpolated from the input sounding to the parcel height at each time step, are used to determine the horizontal motion of the parcels. The two cloud fields in Figs. 16 and 17 were generated on SUN 4/370 in approximately 4 minutes.
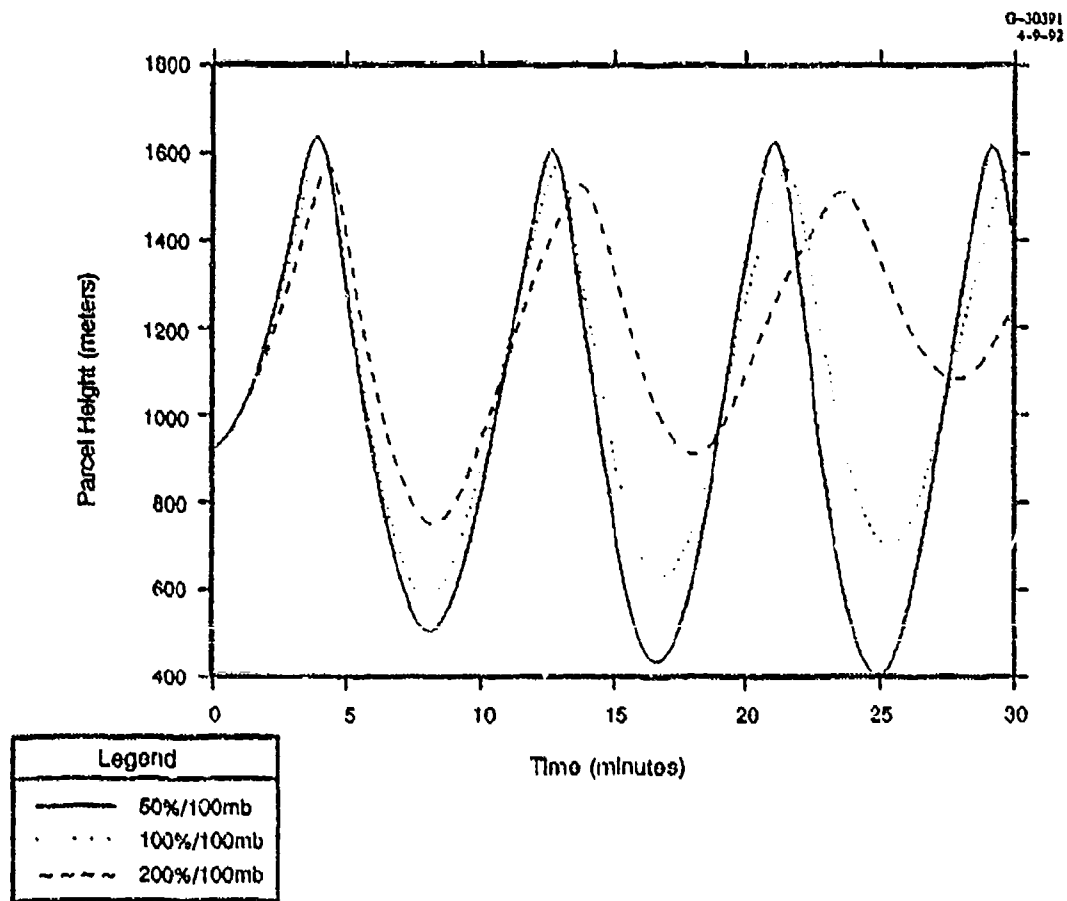
Figure 15 Vertical Position as a Function of Time for 3 Parcels with Different Entrainment Rates

Figure 16 Cumulus Cloud Layer Produced With The Enhanced Cloud Model
(60% Cloud Cover, 10 × 10 km Horizontal Extent)
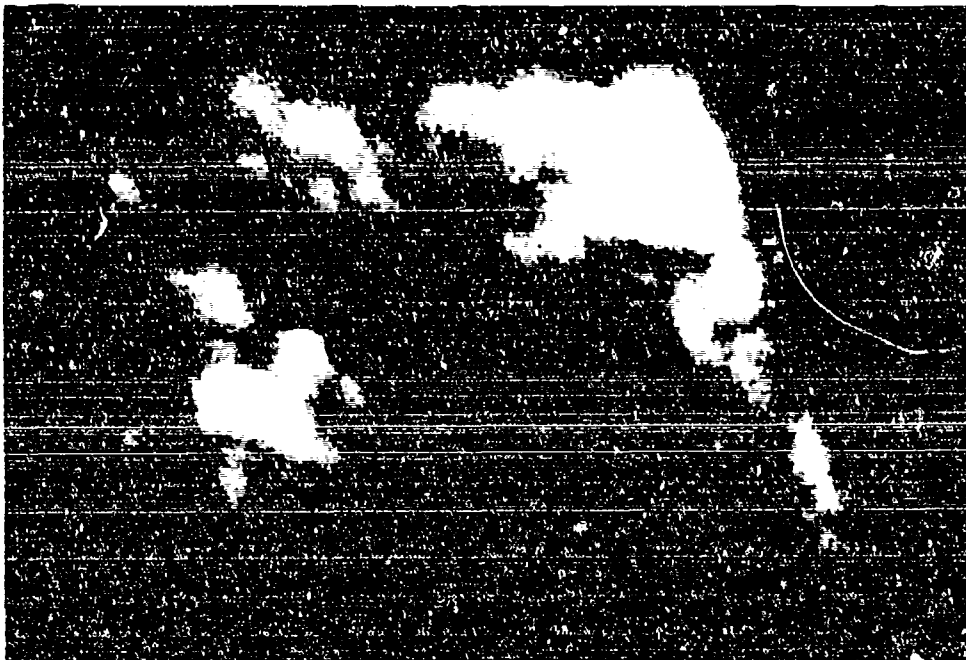
Figure 17 Cumulus Cloud Layer From The Previous
Figure 3 Minutes Later

3. SUMMARY AND RECOMMENDATIONS FOR FUTURE WORK

3.1 SUMMARY

The enhanced cloud scene simulation model, developed under the SWOE program, is an efficient and portable tool to generate multi-layer cloud scenes containing stratiform, cirriform and cumuliform cloud types. Cloud scenes consist of 4-d fields of LWC values and may be used as input to other SWOE models such as those for thermal and radiative transfer.

This report describes four aspects of the enhanced cloud model that were developed since delivery of the interim model: variable-resolution output grid, new fractional Brownian motion algorithm, temporal evolution and a cumulus convection model. This report also contains sample visualizations of cloud model output for a variety of differing model parameters.

In the Interim Technical Report, we described the overall model design and development process. We detailed the major model function and discussed two supporting software packages that use cloud model output fields: one to generate a binary (shadow/no shadow) map for a user-specified date, time and location, and a second to convert 3-d LWC fields to colored polygons to use in scene visualization. That document also presented results from qualitative analysis of aircraft measurements of LWC and comparisons with model-produced data. Taken together, the two reports document technical findings and development made during the cloud scene model development project.

3.2 RECOMMENDATIONS

Throughout model development we emphasized a highly modular software design that would not only accommodate maintenance of the cloud model, but also allow for future growth. Below we list a few recommendations for validation of the current cloud model and suggestions for future growth.

Validate Current Model and Parameters — Limited validation of the cloud model was performed previously in the project and reported in Ref. 1. In that study we compared

model-produced data with aircraft measurements taken near the Hunter-Liggett, California SWOE demonstration site. Results of the comparison were promising, showing good qualitative agreement between the model and measured LWC data. We were able to tune the SRA model parameters to emulate the internal variability of the observed data that followed approximately fractional Brownian motion. A larger validation effort is required to study the appropriateness of a fBm model to simulate other cloud types and clouds from different regions.

Likewise, we recommend comparing the model-produced spatial distribution of cloud elements and their shapes and characteristics with satellite data as a means to obtain improved estimates for the Hurst and resolution parameters that control the cloud/no cloud field generation. Estimates are currently based on studies found in the literature (e.g., Ref. 10) and visual evaluation of cloud fields.

Evaluate Alternative Field-Generation Algorithms — To incorporate the variable-resolution capability in the enhanced cloud model, it was necessary to replace the SRA algorithm with another algorithm that allows point-wise field evaluation. Several models were considered (turning bands (Ref. 17), Boehm sawtooth wave (Ref. 18), etc.), but only one, the RSA model, was implemented due to time considerations. We chose the RSA model because it had been shown to approximate fBm (like the SRA algorithm) and it was highly efficient and flexible. Future model development could involve evaluating alternative models, fBm models or otherwise, for efficiency and suitability to simulate LWC distributions. An important part of that evaluation would be both qualitative and quantitative comparison of model-produced data with LWC measurements.

Extend Cumulus Model — The cumulus model simulates visually realistic cloud scenes with great efficiency and necessarily, many simplifying assumptions. In the future, modifications to the cumulus model that would *not* require great increases in computational time could include: introducing a more sophisticated treatment of the entrainment model to account for parcel interactions and the temporal life-cycle of cumulus fields and adding a precipitation model for greater realism

A higher level of sophistication could be added by reformulating the current model, which is based on hydrostatic stability alone, to include the equations of motion (including

viscosity and diffusion terms) and the continuity equation as ordinary differential equations (ODEs). We could then employ one of the many available ODE solvers to find the position and state of parcels as a function of time.

Model Precipitation and Humidity Fields — The enhanced cloud model was developed specifically to simulate cloud fields. Future efforts could expand the fundamental field generation capabilities developed under this project to simulate corresponding humidity and precipitation fields as well. Through analyzing empirical data, we could fine-tune the model parameters to synthesize cloud moisture based on a variety of data sources (e.g., radar echoes, satellite data, rawinsonde, etc.).

Model radiative properties — A natural extension of the cloud modeling work is integration with existing radiative transfer codes (e.g., LOWTRAN7). A goal of the integration would be to use the high-resolution cloud fields generated with the cloud model to enable high-resolution radiative computations. To offset the increases in computational time due to the increased resolution, we could employ variable-resolution data structures (octrees, quadtrees, etc.) and efficient ray-tracing methods developed for visualization of semi-transparent media.

Future efforts could also include modeling drop-size distributions along with the water density fields that the model currently produces. The model distributions could then be used in cloud scene visualization in different wavelength bands (e.g., infrared, millimeter wave and visible). A ray tracing technique could be used to visualize the cloud scenes taking into account transmission, attenuation and other radiative properties of the cloud field.

REFERENCES

1. Cianciolo, M.E., Hersh, J.S., and M.P. Ramos-Johnson, Cloud scene simulation modeling interim technical report, TASC Technical Report TR-6042-1, November 1991, PL-TR-91-2295. (ADA256689)

2. Cianciolo, M.E., Cloud scene simulation model version 3 use and maintenance guide, TASC Technical Information Memorandum, TIM-6042-4, February 1992.

3. Saupe, D., Point evaluation of multi-variable random fractals, in *Visualisierung in Mathematik and Naturwissenschaft*, H. Jurgens and D. Saupe (eds.), Springer-Verlag, Heidelberg, 1989.

4. Feddes, R.G., A synoptic-scale model for simulating condensed atmospheric moisture, USAFETAC-TN-74-4, 1974.

5. Zhang, G.J., and N.A. McFarlane, Convective stabilization in midlatitudes, Monthly Weather Review, vol. 119. August 1991, pp. 1915-1928.

6. Fleagle, R.G., and J. Bassinger, *An Introduction to Atmospheric Physics (Second Edition)*, Academic Press, New York, 1980, Ch. 2.

7. Cotton, W.R., and R.A., Anthes, *Storm and Cloud Dynamics*, Academic Press, San Diego, 1989, Ch. 8.

8. Peitgen, H.O., and D. Saupe, *The Science of Fractal Images*, Springer Verlag, New York, Ch. 2, 1988.

9. Berry, M.V., and Z.L. Lewis, On the Weierstrass-Mandlebrot fractal function, Proceedings of the Royal Society of London, Series A, vol. 370, pp. 459-484, 1980.

10. Cahalan, R.F., and J.H. Joseph. Fractal statistics of cloud fields, Monthly Weather Review, vol. 117, pp. 261-272, 1989.

11. Cahalan, R.F., Overview of fractal clouds, *RSRM '87: Advances in Remote Sensing Retrieval Methods*, pp. 371-389, 1987.

12. Scorer, R.S., and F.H. Ludlam, Bubble theory of penetrative convection, Quarterly Journal of the Royal Meteorological Society, vol. 79, pp. 94-103, 1953.

13. Yau, M.K., and R. Michaud, Numerical simulation of a cumulus ensemble in three dimensions, J. Atmospheric Sciences, vol. 39, pp. 1062-1079, 1982.

14. Hill, G.E., Factors controlling the size and spacing of cumulus clouds as revealed by numerical experiments, J. Atmospheric Sciences, vol. 31, pp. 646-673, 1974.

15. Bolton, D., The computation of equivalent potential temperature, Monthly Weather Review, vol. 108, no. 7, pp. 1047, 1980.

16. Byers, H.R., *General Meteorology*, McGraw-Hill, New York, 1974, Ch. 6.

17. Tompson, A.F.B., R. Ababou, and L..W. Gelhar, Implementation of the three-dimensional turning bands random field generator, Water Resources Research, vol. 25, no. 10, pp. 2227-2243, October 1989.

18. Gringorten, I.I., and A.R. Boehm, The 3D-BSW model applied to climatology of small areas and lines, AFGL-TR-87-0251, 1987, ADA19114.